Eyecharts: Constructive Benchmarking of Gate Sizing Heuristics

[†]Puneet Gupta, [¶]Andrew B. Kahng, [†]Amarnath Kasibhatla, [§]Puneet Sharma
[†] University of California, Los Angeles [¶]University of California, San Diego [§]Freescale Semiconductor
[†]{puneet, amar}@ee.ucla.edu [¶]{abk@cs.ucsd.edu} [§]{puneetsharma@freescale.com}

***Abstract*—Discrete gate sizing is one of the most commonly used, flexible, and powerful techniques for digital circuit optimization. The underlying problem has been proven to be NP-hard [1]. Several (suboptimal) gate sizing heuristics have been proposed over the past two decades, but research has suffered from the lack of any systematic way of assessing the quality of the proposed algorithms. We develop a method to generate benchmark circuits (called *eyecharts*) of arbitrary size along with a method to compute their optimal solutions using dynamic programming. We evaluate the suboptimalities of some popular gate sizing algorithms. Eyecharts help diagnose the weaknesses of existing gate sizing algorithms, enable systematic and quantitative comparison of sizing algorithms, and catalyze further gate sizing research. Our results show that common sizing methods (including commercial tools) can be suboptimal by as much as 54% (V_t-assignment), 46% (gate sizing) and 49% (gate-length biasing) for realistic libraries and circuit topologies.**

Categories and Subject Descriptors: B.7 [Integrated Circuits]: Design Aids
General Terms: Algorithms, Design
Keywords: Gate sizing, benchmarking, dynamic programming

I. Introduction

The *sizing problem* in digital VLSI design seeks to tune the circuit parameters of supply voltage, threshold voltage, gate-length and gate-width to optimize a tradeoff of speed, area and power. The sizing problem arises at all stages of the RTL-to-GDS implementation flow, and even beyond (e.g. [2]). The classical problem of discrete gate sizing is to assign a size (from a pre-characterized cell library) to each gate in a combinational logic block, such that the block's total power is minimized, subject to a maximum delay constraint. Finding the optimal gate sizing solution for a given digital logic circuit can be NP-hard [1].

Fishburn and Dunlop proposed a fast greedy method, TILOS [3], to minimize area while meeting delay constraints. Chan [4] gives a pseudo-polynomial time slack-computation algorithm and a backtracking algorithm for gate sizing. Previous methods have also used mathematical programming techniques to do gate sizing: linear programming (LP) [5]–[8], Lagrangian relaxation [9], [10], and convex optimization [11]–[13]. Other methods include sensitivity-based approaches [2], [14]–[16], dynamic programming (DP) [17], [18] and heuristics guided by continuous programming [19]. Coudert et al. [15] give a good comparison of the gate sizing algorithms proposed during the early 1990s.

None of the previous methods in the literature (except in [20], [21]) quantify their own suboptimality or focus on characterizing and investigating the suboptimalities of existing algorithms. There is no consistent benchmarking methodology when comparing sizing heuristics. Results in [20] show that sensitivity-based and continuous solution-guided approaches are not robust, as their suboptimality varies widely (from 4% to 52%) when applied to different ISCAS-85 benchmarks having nearly identical sizes. A more rigorous approach is needed to characterize and provide insight into the behavior of different algorithms over different classes of input circuits. Suboptimality studies of existing heuristics have already been performed for other VLSI problems such as logic synthesis [22], placement [23], [24] and optimal buffer insertion [25], [26]. However, to our knowledge we are the first to investigate the suboptimalities of gate sizing heuristics in a systematic way.

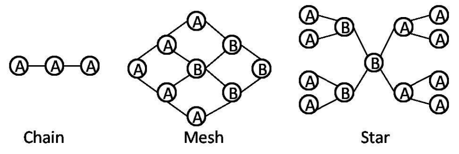

Fig. 1. Basic eyechart topologies.

In this paper, we present a method to generate combinational logic circuits (called *eyecharts*) which are combinations of the basic *chain, mesh* and *star* topologies shown in Figure 1. These eyecharts, together with their optimal solutions, can be used to benchmark gate sizing heuristics. The idea is to test *just* gate sizing heuristics and not any structural/logic optimization heuristics. Our contribution is especially useful in benchmarking the heuristics which are often used during post-layout optimization phase where gate sizing, Vt-assignment, gate-length biasing are the main choices. We note that the basic eyechart topologies in Figure 1 represent the common elements of real circuits. For example, Figure 2 shows a half-adder circuit which has similarities to a multi-output mesh topology. Our benchmarks can be generated with various complexities and topologies (in terms of fanout, logic depth, and the number of primary inputs (PIs) and primary outputs (POs)) to study the behavior of existing algorithms under such variations. This helps us identify the weaknesses of existing algorithms and may help predict the behavior of a given heuristic or algorithm for a given arbitrary circuit. Our experiments show that the suboptimalities of popular sizing methods can be as large as 54%.[1]

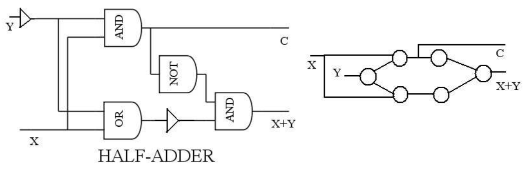

Fig. 2. The half-adder with buffers, with its corresponding graph shown on the right, is similar to a multi-output mesh topology, which is an extended version of the basic mesh topology, and is discussed in Section III.

The contributions of our paper are:

- a set of basic combinational logic topologies that we call eyecharts;
- a method to size the gates in the eyecharts optimally using DP;
- a method to form arbitrarily large combinational logic circuits by daisy-chaining the proposed basic topologies, while retaining the ability to optimally size these circuits; and

[1]Without loss of generality, we only present the details for leakage optimization in this work.

- experiments and results that show the suboptimality behavior of commonly used gate sizing methods under varied topological, delay/power modeling as well as optimization contexts.

The organization of our paper is as follows. Section II describes our method to optimally solve the basic eyechart topologies. Section III describes the method to construct and solve larger *hybrid eyecharts* (formed by daisy-chaining basic eyecharts). Section IV describes the details of our experimental setup for the suboptimality studies. Section V reports the results of several suboptimality case studies using five sizing heuristics (including two commercial tools).

II. Solving Basic Eyechart Topologies

In this section, we present a method to perform optimal sizing of the basic eyechart topologies shown in Figure 1 using DP. Optimally solving a chain topology entails allocation of a delay budget to each *stage* such that the total power is minimized. Here, stage refers to the level of the logic gate, with PIs at the first level or stage. The delay budget assignment (without output load dependence) is essentially a multi-stage allocation problem which can be solved optimally using DP [27].

For an N-stage chain, the DP recursion is shown in Equations 1 and 2. We assume that a gate's delay depends only on its size and its total output capacitance. We assume that each gate has k discrete sizes. D_{max} denotes the maximum delay constraint, $C(s)$ is the input capacitance of an inverter of size s, p_{ij} and $d_{ij}(C(s))$ respectively indicate the leakage power and delay (for an output capacitance $C(s)$) of the gate at stage i with size j. Let x_i denote the cumulative delay budget for stage i; then the total power (for an output load $C(s)$) through stage i is denoted by $P_{i,C(s)}(x_i)$.

$$P_{1,C(s)}(x_1) = \min_j\{p_{1j}\} \text{ s.t. } d_{1j}(C(s)) \le x_1,\ 1 \le j \le k,\ 1 \le s \le k \qquad (1)$$
$$\min_j\{d_{1j}(C(s))\} \le x_1 \le D_{max}$$

$$P_{i,C(s)}(x_i) = \min_j\{p_{ij} + P_{i-1,C(j)}(x_i - d_{ij}(C(s)))\} \text{ s.t. } d_{ij} < x_i \qquad (2)$$
$$1 \le j \le k,\ 1 \le s \le k$$
$$\min(x_{i-1}) + \min_j\{d_{ij}(C(s))\} \le x_i \le D_{max},\ \text{for } i \le 2 \le N-1$$
$$\text{and } x_N = D_{max}$$

For any stage i, the optimal size for a given cumulative delay budget is determined by an exhaustive local search among the available gate sizes. This is done for all of the possible output loads seen by stage i due to stage $i+1$. Stage $i+1$ is then solved optimally by considering all of its gate size choices and the stage i's optimal size (for an output load equal to stage $i+1$'s input capacitance) for the range of cumulative delay budgets shown in Equations 1 and 2. It is easy to see that the problem has an optimal substructure.[2] Dynamic programming therefore solves this sizing problem optimally. Note that the principle of optimality holds *only* if the delay of stage i depends only on the input capacitance of stage $i+1$. This "levelization" of the circuit graph is the key for preserving optimality.

We observe that for each stage, an optimal gate size entry exists for all possible cumulative delay budgets and for all possible output loads. The last stage's cumulative delay budget table has only one entry corresponding to the given PO load capacitance and the maximum delay constraint (since optimal sizing uses the full delay budget). A DP execution for a three-stage inverter chain, with the delay model shown in Table I, is shown in Table II (CP denotes cumulative power, OS denotes optimal gate size).

After constructing the table, the optimal size for each stage is found by traversing the cumulative delay budget table backwards from PO to PI and allocating a delay budget (and therefore a size) to each stage. The bolded values in Table II show this.

The mesh and star topologies are optimally solved by first reducing them to chains. This is shown in Figure 3 and Figure 4. A stages with

[2]Consider an n-stage chain not containing the optimal solution for $n-1$ stages with the given output load. In that case, the solution can be improved by substituting the optimal solution for stage $n-1$.

TABLE I
Delay Table for the Inverter Used in the Numerical Example.

	Input cap	Leakage power	Delay	
			Load cap 3	Load cap 6
Size 1	3	5	3	4
Size 2	6	10	1	2

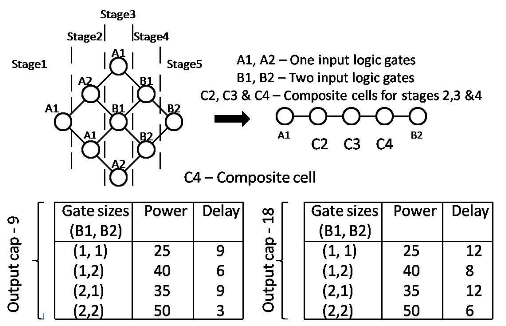
Stage3
Stage2
Stage4
Stage1
Stage5
A1
A2
B1
A1
B1
B2
A1
B2
A2
A1, A2 – One input logic gates
B1, B2 – Two input logic gates
C2, C3 & C4 – Composite cells for stages 2,3 &4
A1
C2
C3
C4
B2
C4 – Composite cell
Output cap - 9
Output cap - 18

Output cap - 9

Gate sizes (B1, B2)	Power	Delay
(1, 1)	25	9
(1,2)	40	6
(2,1)	35	9
(2,2)	50	3

Output cap - 18

Gate sizes (B1, B2)	Power	Delay
(1, 1)	25	12
(1,2)	40	8
(2,1)	35	12
(2,2)	50	6

Fig. 3. Mesh to chain reduction. All values for B1 and B2 are assumed to be twice and thrice, respectively, that of the values shown in Table I.

two or more gates is represented using a *composite cell*, to capture the power and delay characteristics of all the gates in that stage. A composite cell of a stage is a tabular representation that has power and delay values for all the possible gate size combinations of all the gates belonging to that stage, for all the possible output load combinations. For example, if A1, A2, B1 and B2 each have two gate sizes, then the composite cell of stage 3 will have $2^3\{A_1, B_1, A_2\} \times 2^2\{B_1, B_2\}$ entries. Since each stage with multiple gates is enumerated for all the possible output loads, *we preserve optimality in this reduction even if the gates belonging to a stage are non-homogeneous.* The gate size entry and the input capacitance entry of a composite cell is a vector of gate sizes and input capacitances respectively, of each gate in that stage. For a gate size of a composite cell, the power is the sum of the powers and the delay is the maximum of the delays, of the individual gates. An example of this is shown for stage 4 of the mesh topology in Figure 3. The composite cell *C4* represents the gate size vector, power and delay values of the gates of stage 4.

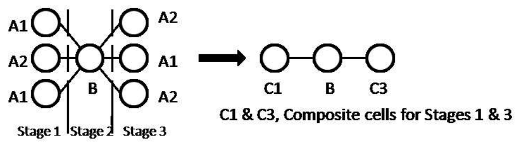

Fig. 4. Star to chain reduction.

III. Optimal Sizing of Hybrid Eyecharts

We generate large hybrid eyecharts by daisy-chaining the basic chain, mesh and star topologies. In this section, we explain how to optimally solve the hybrid eyecharts.

A. Hybrid Benchmarks Constructed with Basic Topologies

We solve a hybrid eyechart by reducing it to a simple chain using a process similar to the one described in Section II. Figure 5 shows a sample hybrid eyechart and its reduced chain equivalent. While creating a hybrid eyechart, we mark each gate in the circuit with a tag that indicates whether it belongs to a chain, mesh or star structure. All the stages that belong to a mesh are reduced to single cells using composite cell models. Starting from each PI, we build cumulative delay budget tables for each stage until the star node in the center (gate C in Figure 5) is reached. For each such PI chain, the cumulative delay budget table of the last stage has cumulative power values for different cumulative delay budgets for the whole PI chain. Now, these PI chains in parallel can be represented using a single composite cell, as with Chains 1 and 2 in the hybrid eyechart of Figure 5. The entries for the power of this cell for each budget will be the sum of the individual powers of each PI chain.

TABLE II
NUMERICAL EXAMPLE FOR A THREE-STAGE INVERTER CHAIN . THE FINAL OPTIMAL SIZING SOLUTION IS SHOWN IN **bold** FONT.

Output cap	Stage 1			Stage 2			Stage 3		
	Budget	CP	OS	Budget	CP	OS	Budget	CP	OS
3	**1**	**10**	**2**	3	20	2			
3	2	10	2	**4**	**15**	**1**			
3	3	5	1	5	15	2			
3	4	5	1	6	10	1			
3	5	5	1	7	10	1			
3	6	5	1	8	10	1			
3	7	5	1						
3	8	5	1						
6	2	10	2	4	20	2	**8**	**20**	**1**
6	3	10	2	5	15	1			
6	4	5	1	6	15	2			
6	5	5	1	7	10	1			
6	6	5	1	8	10	1			
6	7	5	1						
6	8	5	1						

Budget tables are built for each stage of the Chains 3 and 4 by following the same steps taken for the PI side chains, allowing them to be represented using a single composite cell. The whole circuit can now be treated as a chain and solved using the DP recursion described in Section II. To determine the optimal sizes for all the gates in the circuit, the delay budgets allocated to each cell of the reduced chain are applied to the corresponding PI/PO chains. The stages with only one gate are assigned gate sizes directly from the cumulative budget table, and the gate sizes for other stages are assigned from the entries found in their respective composite cell tables.

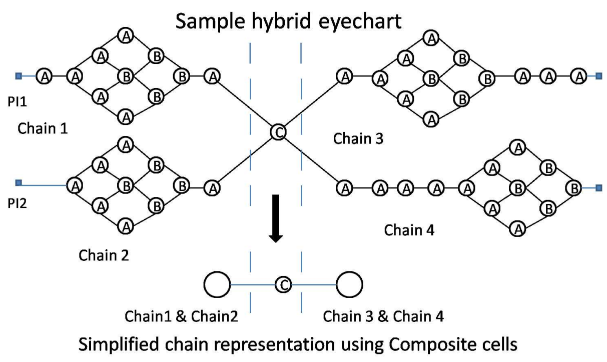

Fig. 5. Hybrid eyechart reduced to a chain.

B. More General Eyechart Topologies

Topologies that are more complex than the basic eyechart topologies can also be solved. We illustrate this with a multi-output mesh topology, as shown in Figure 6. This topology has two two-input cells added in the last stage. A unique property of the three basic eyechart topologies, unlike the multi-output mesh, is that a gate at any stage i has inputs coming only from stage $i-1$ and its fanout goes only to gates in stage $i+1$. We treat the group of stages which do not satisfy this unique property as a single stage and solve it using local enumeration. For example, in Figure 6, stages three, four and five are treated as a single stage (enclosed by a box), which is enumerated. The rest of the circuit is solved using the method described in Section II. Other similar topologies can be added (albeit at the cost of optimization runtime) in the same way, which can make our eyechart approach fairly flexible.

IV. IMPLEMENTATION DETAILS AND EXPERIMENTAL SETUP

A C++ program has been written which generates and solves these eyecharts, and which also writes out their corresponding netlists, parasitics and delay models in the industry-standard .v, .spef and .lib formats so that they can be easily used with standard sizing tools. The complexity of the DP recursion described in Section II is bounded by $O(P \cdot N \cdot B \cdot k^n)$, for a circuit with P PIs/POs, N stages, delay

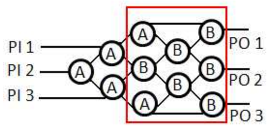

Fig. 6. Multi-output mesh topology.

budget B, k sizes per gate and n gates per stage. Solving a hybrid benchmark circuit with 10,000 gates takes approximately four hours.[3]

Delay tables are formed with delay entries for all possible output load combinations, to avoid interpolation. This makes the number of capacitance indices for the delay tables dependent on the maximum fanout in the circuit. For example, if the library has three sizes per standard cell and the maximum fanout in the circuit is three, then the delay table would have nine capacitance indices. This ensures that any combination of output loads will fall in the range of available discrete capacitance entries in the delay table. To test the suboptimalities of post-routing leakage optimization tools, we also insert parasitic capacitances at different nodes. The values of the parasitic capacitances are set to be integral multiples of a minimum constructed gate capacitance so that the total load capacitance seen by a gate has a corresponding index in the delay table. To preserve optimality, we ignore some complexities (e.g., crosstalk, slew propagation, etc.), which are handled by practical optimization engines.

We experimented with the following five different gate sizing methods for suboptimality studies.

- *Comm1, Comm2*: Two well known commercial gate sizing and leakage optimization tools. Unfortunately, we do not know the internal details of these optimizers.
- *LP*: A linear programming-based slack allocation and sizing tool which is an implementation of [7]. First, it optimizes the circuit for maximum speed. Then, it uses power-delay sensitivities in a linear programming-based slack allocation to maximize the power savings. It uses a freely distributed linear programming solver *lp_solve* (http://lpsolve.sourceforge.net/5.1).
- *GS*: A greedy sensitivity-based sizing tool similar to [2], [16] but with a TILOS [3]-like sensitivity function ($\Delta power/\Delta delay$).
- *SBS*: A sizing tool that uses the slack-based greedy sensitivity metric ($\Delta power/\Delta slack$) proposed in [2], [16].

Note that all the above heuristics except LP use an incremental timing engine in the optimization loop. Due to delay modeling approximations, LP can sometimes violate timing constraints. We pick the delay constraint values (by trial and error) that LP can achieve and run the rest of the heuristics (as well as the optimal DP) with those constraints. This ensures that all our comparisons are fair in terms of suboptimality, but a practical LP-based optimizer will need additional hooks to fix timing violations.

The following four types of delay and power tradeoffs with size are investigated.

- LP-LD: Linear increase in power with size and a linear fit of delay to size/load.
- LP-NLD: Linear increase in power with size and a nonlinear fit of delay to size/load.
- EP-LD: Exponential increase in power with size and a linear fit of delay with size/load.
- EP-NLD: Exponential increase in power with size and a nonlinear fit of delay to size/load.

In the EP-LD and EP-NLD models, we use the term "cell-variant" to indicate that the cell swapping choices are V_t or gate-length variants. We assume that the input capacitance of a gate remains the same across V_t variants. For gate-length variants, the capacitance increases linearly with gate-length. All the delay values were fitted individually for each type of standard cell, using an industrial multi-V_t 65 nm CMOS technology library. Table III gives a summary of

[3]Note that this runtime is not a huge concern since the DP method is not intended for use in practical optimization, but only for benchmarking.

the characteristics of the four library models used in our experiments, along with the corresponding optimization contexts.

Table III shows the RMS error of each of these fits. Power values for all four library models are taken from the reference technology library and hence do not involve fitting (except for the studies which involve more number of sizes/variants than the listed default number). The minimum delay budget for any benchmark is found by maximally sizing all the gates in the design.[4]

TABLE III
SUMMARY OF LIBRARY MODEL CHARACTERISTICS.

Library model	RMS fitting error (delay)	Optimization context	Default # sizes/variants
LP-LD	8.43%	Gate sizing	8
LP-NLD	0.3%	Gate sizing	8
EP-LD	8.43%	V_t , gate-length bias	3, 3
EP-NLD	0.3%	V_t , gate-length bias	3, 3

V. SUBOPTIMALITY CASE STUDIES

In this section we present the results of a few interesting case studies that compare the suboptimalities of the five optimization heuristics outlined in Section IV. These studies are by no means exhaustive and many other experiments are possible using eyecharts as a diagnostic tool. All of the suboptimality values are calculated as

$$\text{Suboptimality\%} = \frac{\text{method\_power} - \text{optimal\_power}}{\text{optimal\_power}} \times 100. \qquad (3)$$

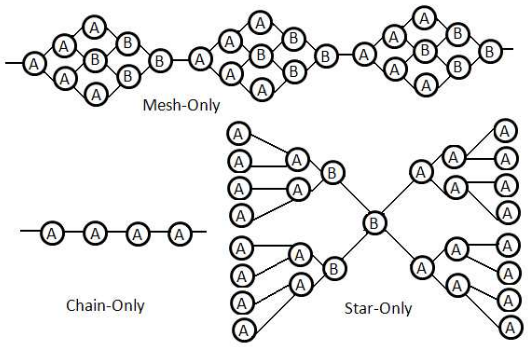

Fig. 7. Daisy-chained individual topologies.

A. Dependence on Circuit Topology

Figure 7 illustrates large chain-, mesh- and star-only circuits obtained by daisy-chaining the basic topologies. We fix the netlist size at approximately 10,000 gates and perform the optimizations with varying delay constraints. The average fanin/fanout depends on the length of the mesh (three-stage, five-stage etc., mesh), maximum fanin of the star-only cells, and total number of stages in the daisy chain. The average fanouts (and fanins, due to symmetry) of chain-, mesh- and star-only topologies used in this experiment and shown in Figure 7 are 1, 1.875 and 1.95 respectively. Figure 8 shows the suboptimalities for mesh and star topologies; these results indicate that a mesh structure is more difficult to solve than a star structure. With respect to circuit topology, *designers should look out for mesh-like topologies (i.e., with reconvergent fanouts) since none of the tested heuristics perform well on them.*

We also studied the impact of circuit size on suboptimality. We varied the circuit's logic depth and number of PIs/POs, while keeping the topology of the hybrid eyechart the same as in Figure 5. The corresponding results (on benchmarks with sizes ranging from 100 to 51,500 gates) show that the suboptimality is unaffected by the size of the design, and hence for the rest of the studies, we use a hybrid benchmark with 10,000 gates.

[4]Note that this may not be the fastest possible implementation for the case of gate sizing, where the dependence of the circuit delay on individual gate sizes is not necessarily monotone.

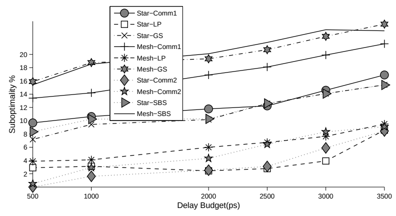

Fig. 8. Suboptimality comparison of the daisy-chained mesh-only and star-only topologies. The chain-only suboptimality results show that all the compared methods have close to zero suboptimalities and hence are not shown.

B. Effect of Delay Modeling

We compare the delay models using a single hybrid benchmark with 10,000 gates. This benchmark has a topology similar to the sample hybrid eyechart of Figure 5 with a multi-output mesh topology added at each of the POs. It has four PIs and five POs. 1,000 five-stage mesh topologies and inverter chains are also inserted randomly into the benchmark. INV, NAND and four-input AOI gates, each with eight discrete gate sizes, are used.

We experimented with the LP-LD delay model and the suboptimality results are shown in Figure 9. *Comm2* has the best suboptimality, while *LP* performs much better than the three remaining optimizers. This is expected since linear power-delay tradeoffs are better suited for the LP-based slack-allocation engine. To evaluate the performance

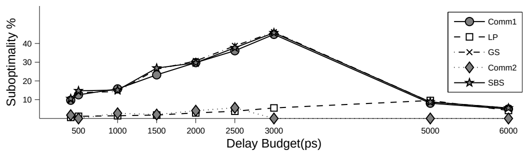

Fig. 9. Suboptimalities for LP-LD model.

of the chosen optimizers with realistic delay models, .lib models are generated with the LP-NLD delay model. Figure 10 shows the corresponding suboptimality trends. Note that the delay dependence on size is only weakly nonlinear in the 65 nm library used in this paper. The performance of the *LP* and *Comm2* methods suffers under the nonlinear delay model while that of *Comm1*, *SBS* and *GS* improves, especially with relaxed timing constraints. A possible reason is the ability of *Comm1*, *SBS* and *GS* to exploit the nonlinearity. Without

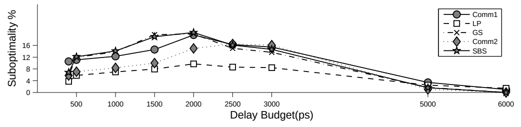

Fig. 10. Suboptimalities for LP-NLD model.

knowing the details of *Comm1* and *Comm2*, one conclusion we can draw is that even with the nonlinearity in the commercial delay tables, *linear programming is a good approach for linear power tradeoffs.*

The non-monotone trends in the suboptimalities can be explained using Figure 11. The *suboptimality of any of the compared methods is the least for both the smallest and the largest delay budgets, while the optimal power decreases with increasing delay budget.* This results in the observed non-monotone behavior of the suboptimalities.

C. Effect of Library Granularity

We experimented with a varying numbers of gate sizes for the LP-NLD model. For these experiments, the delay and power ranges are kept the same as in Section V-B while the granularity in gate sizes is increased. Figure 12 shows the corresponding trends in suboptimality. It can be seen that the performance of *Comm1* and *Comm2* are relatively unaffected while *LP's suboptimality improves noticeably,*

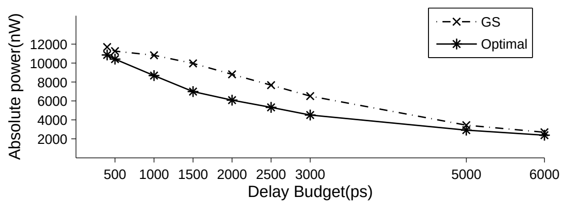

Fig. 11. Absolute power comparison for LP-LD model.

which is likely due to a smaller error in snapping the continuous solution to a discrete one.

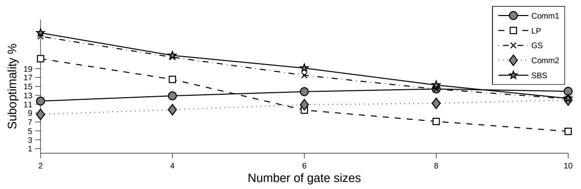

Fig. 12. Suboptimalities vs. number of gate sizes for LP-NLD model with 1500 ps delay budget.

For the same experiment, Figure 13 shows the optimal power values for different delay budgets with two, four and six gate sizes, normalized to the optimal power values with eight gate sizes. Since the delay range is the same for these experiments, higher granularities create more gate sizing options for smaller delay increments. Hence, *a higher library granularity results in a lower optimal power, but the difference is not very pronounced*.

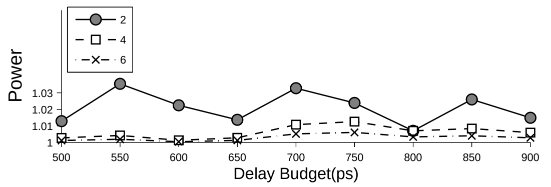

Fig. 13. Optimal power vs. delay budget for different gate size granularities. Power values are normalized to corresponding optimal results for eight gate sizes.

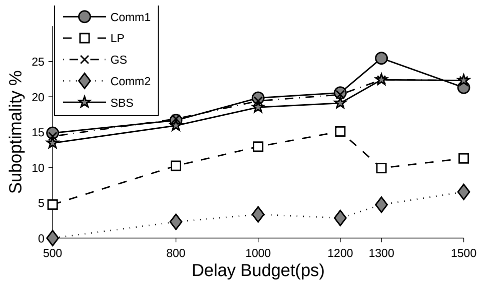

Fig. 14. Suboptimalities for EP-LD model under different delay constraints, using V_t variants only.

D. The V_t-assignment Context

We experimented with the EP-LD and EP-NLD library models by varying the delay constraint for the case where each cell has three variants. The corresponding results are shown in Figure 14 and Figure 15 respectively. The minimum delay budget for optimization is found by assigning low V_t variants to all of the cells. *LP* and *Comm2* perform relatively well for the smaller budgets but their suboptimality increases for the larger delay budgets. Moreover, the suboptimality difference between the LD and NLD delay modeling is more pronounced for the *LP* optimizer.

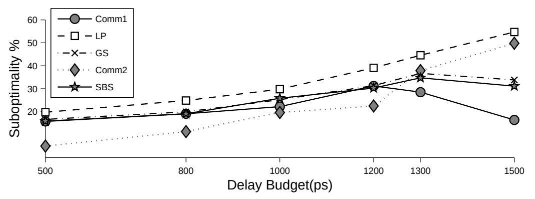

Fig. 15. Suboptimalities for EP-NLD model using V_t variants only.

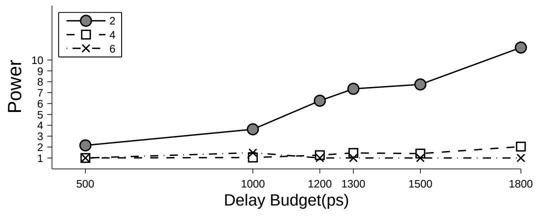

Fig. 16. Optimal powers for varying delay budgets and different V_t granularities. The powers are normalized to the corresponding results for eight V_t variants.

Figure 16 shows the optimal power values for different delay constraints for two, four and six V_t variants, normalized to the powers with eight V_t variants.[5] Since the delay range is the same for these experiments, higher granularities create more V_t options for smaller delay increments, resulting in lower optimal powers. These results suggest a *strong benefit in increasing the number of cell variants when the power tradeoff is exponential*, in contrast to the case in Figure 13, which has a linear power tradeoff.

E. The Gate-length Biasing Context

Figure 17 shows the trends for gate-length biasing. Gate-length variants have different input capacitance values as opposed to V_t variants. In these results, all of the tools perform worse than the gate sizing or V_t-assignment cases. This is especially true for *LP* whose suboptimality rises to over 40% and it does not perform better than the simple GS and SBS approaches. Iterative methods like *GS* and *SBS*, which use a real static timing engine, perform better than *LP* due to the near-quadratic dependence of the delay on the gate-length. This near-quadratic dependence is due to the reduced drive strength of the driver, and the increased input capacitance of the load, for an increased gate-length.

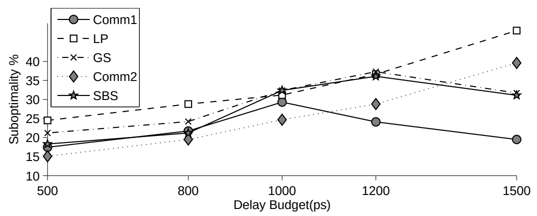

Fig. 17. Suboptimalities for EP-NLD model using gate-length variants only.

F. Observations

We summarize our main observations and conclusions below.

- All of the tools fare well on designs with low fanouts (i.e., designs that are topologically close to the chain eyechart).
- All of the tools fare poorly on designs with reconvergent fanouts (i.e., designs that are topologically similar to the mesh eyechart).
- For gate sizing and V_t-assignment, linear programming-based solvers can perform surprisingly well. Their solution quality

[5]We realize that more than three V_ts are rarely used in practice. Nevertheless, we show the results with more variants to highlight what is achievable.

suffers significantly in the gate-length biasing context where the delay is a strongly nonlinear function of the gate-length.

- The commercial tools do well in different optimization contexts (but unfortunately we cannot offer more insight here). These tools, as well as the sensitivity-based sizers *GS* and *SBS*, benefit from not needing to fit a closed-form delay/power model to real library data.
- The benefits of having a finer granularity in a library is much more pronounced for exponential power tradeoffs (such as gate-length biasing and V_t-assignment) than linear power tradeoffs (as in the case of gate sizing).
- Local sensitivity-based heuristics like *GS* and *SBS* can be highly suboptimal for large delay budgets due to their tendency to be trapped in local minima (as we have seen with star or mesh topologies).

VI. Extensions to Complex Delay Models

Finally, we have also applied our approach to a slew-dependent delay model. In this case, we assume that a gate's delay depends on the input slew and the load capacitance, while the output slew of a gate depends only on its size and the load capacitance. Unfortunately, in this case our method cannot guarantee optimality due to the need to maintain the slew and load consistency while building the tables. The method to solve a chain for the slew-dependent delay model is the same as the method described in Section II, except that a 3D budget table is used for each stage, with the input slew, the output load and the delay budget as the three indices. We take the best of the forward propagation (as in Section II with fixed PO load capacitance) and the reverse propagation (i.e., fixed PI slew). For the mesh and star structures, we first build composite cells for all the input slew and output load combinations and then solve them in the same manner as we solve a chain. Even though this method may not be optimal, the experimental results in Figure 18 show that the existing methods used for comparison are still considerably worse. We realize that a realistic delay model has slew and signal integrity dependence. Nevertheless, we believe that our work has made a significant contribution in highlighting the huge suboptimalities of the sizing heuristics studied, as well as the dependence of these suboptimalities on the circuit topology and the delay-size and power-size tradeoffs. However, we believe that our work is a significant contribution in highlighting the huge suboptimalities of the compared sizing heuristics and the dependence of the suboptimalities on the circuit topology and the delay-size and power-size tradeoffs.

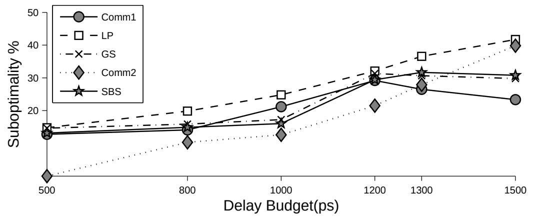

Fig. 18. Suboptimalities for EP-NLD model with slew-dependent delay model.

VII. Conclusions and Future Work

We have described a method to generate arbitrarily large circuits with known optimal solutions that can be used to benchmark and diagnose the problems with sizing heuristics. The benchmarks and the code can be downloaded from http://nanocad.ee.ucla.edu/Main/DownloadForm. We have studied the optimization contexts of gate sizing, V_t-assignment and gate-length biasing with two commercial and three academic sizing heuristics. Our results show that these heuristics can be suboptimal by as much as 54%. The context of gate-length biasing has the worst suboptimality overall, with a minimum suboptimality of 14%. Also, the presence of reconvergent fanouts in a circuit topology results in a greater suboptimality compared to a similar topology without reconvergent fanouts. We also note that linear programming-based methods perform well under most scenarios, while local sensitivity (TILOS-like)-based heuristics perform better under exponential power-size tradeoffs.

Ongoing studies include generating hybrid eyecharts according to given fanin/fanout and path-length distributions that are derived from real designs. We also plan to detect the presence of the basic eyechart topologies in real designs and measure the similarity of the designs to eyecharts with pre-characterized suboptimalities. This will enable the estimation of suboptimality of a given heuristic on a given design, possibly allowing optimization tools, which implement a collection of sizing heuristics, to choose one at runtime.

References

[1] W. N. Li, "Strongly NP-Hard Discrete Gate Sizing Problems," *Proc. ICCD*, pp. 468–471, 1993.

[2] P. Gupta, A. B. Kahng, P. Sharma, and D. Sylvester, "Gate-length Biasing for Runtime-leakage Control," *IEEE Trans. on CAD*, pp. 1475–1485, 2006.

[3] J. Fishburn and A. Dunlop, "TILOS: A Posynomial Programming Approach to Transistor Sizing," *Proc. ICCAD*, pp. 269–273, 1985.

[4] P. K. Chan, "Algorithms for Library-specific Sizing of Combinational Logic," *Proc. DAC*, pp. 353–356, 1990.

[5] M. R. C. M. Berkelaar and J. A. G. Jess, "Gate Sizing in MOS Digital Circuits with Linear Programming," *Proc. EURO-DAC*, pp. 217–221, 1990.

[6] K. Jeong, A. B. Kahng, and H. Yao, "Revisiting the Linear Programming Framework for Leakage Power vs. Performance Optimization," *Proc. ISQED*, pp. 127–134, 2009.

[7] D. Nguyen, A. Davare, M. Orshansky, D. Chinnery, B. Tompson, and K. Keutzer, "Minimization of Dynamic and Static Power Through Joint Assignment of Threshold Voltages and Sizing Optimization," *Proc. ISLPED*, pp. 158–163, 2003.

[8] A. Srivastava, "Simultaneous Vt Selection and Assignment for Leakage Optimization," *Proc. ISLPED*, pp. 146–151, 2003.

[9] H. Tennakoon and C. Sechen, "Gate Sizing Using Lagrangian Relaxation Combined with a Fast Gradient-based Pre-processing Step," *Proc. ICCAD*, pp. 395–402, 2002.

[10] C.-P. Chen, C. C. N. Chu, and D. F. Wong, "Fast and Exact Simultaneous Gate and Wire Sizing by Lagrangian Relaxation," *Proc. ICCAD*, pp. 617–624, 1998.

[11] S. S. Sapatnekar, V. B. Rao, and P. M. Vaidya, "A Convex Optimization Approach to Transistor Sizing for CMOS Circuits," *Proc. ICCAD*, pp. 482–485, 1991.

[12] K. Kasamsetty, M. Ketkar, and S. S. Sapatnekar, "A New Class of Convex Functions for Delay Modeling and its Application to the Transistor Sizing Problem," *IEEE Trans. on CAD*, pp. 779–788, 2000.

[13] H. Tennakoon and C. Sechen, "Efficient and Accurate Gate Sizing with Piecewise Convex Delay Models," *Proc. DAC*, pp. 807–812, 2005.

[14] O. Coudert, "Gate Sizing for Constrained Delay/Power/Area Optimization," *IEEE Trans. on VLSI Systems*, pp. 465–472, 1997.

[15] O. Coudert, R. Haddad, S. Manne, and S. Manne, "New Algorithms for Gate Sizing: A Comparative Study," *Proc. DAC*, pp. 734–739, 1996.

[16] S. Sirichotiyakul, T. Edwards, C. Oh, R. Panda, and D. Blaauw, "Duet: an Accurate Leakage Estimation and Optimization Tool for Dual-Vt Circuits," *IEEE Trans. on VLSI Systems*, pp. 79–90, 2002.

[17] S. Hu, M. Ketkar, and J. Hu, "Gate Sizing For Cell Library-Based Designs," *Proc. DAC*, pp. 847–852, 2007.

[18] Y. Liu and J. Hu, "A New Algorithm for Simultaneous Gate Sizing and Threshold Voltage Assignment," *Proc. ISPD*, pp. 27–34, 2009.

[19] S. S. Shah, A. Srivastava, V. Zolotov, D. Sharma, D. Sylvester, and D. Blaauw, "Discrete Vt Assignment and Gate Sizing Using a Self-snapping Continuous Formulation," *Proc. ICCAD*, pp. 705–711, 2005.

[20] T.-H. Wu and A. Davoodi, "PaRS: Fast and Near-optimal Grid-based Cell Sizing for Library-based Design," *Proc. ICCAD*, pp. 107–111, 2008.

[21] H. Ren and S. Dutt, "A Network-Flow Based Cell Sizing Algorithm," *Proc. IWLS*, pp. 7–14, 2008.

[22] I. L. Markov and J. A. Roy, "On Sub-optimality and Scalability of Logic Synthesis Tools," *Proc. IWLS*, 2003.

[23] J. Cong, M. Romesis, and M. Xie, "Optimality and Stability Study of Timing-Driven Placement Algorithms," *Proc. ICCAD*, pp. 472–478, 2003.

[24] L. W. Hagen, D. J.-H. Huang, and A. B. Kahng, "Quantified Suboptimality of VLSI Layout Heuristics," *Proc. DAC*, pp. 216–221, 1995.

[25] J. Lillis, C.-K. Cheng, and T.-T. Y. Lin, "Simultaneous Routing and Buffer Insertion for High Performance Interconnect," *Proc. GLSVLSI*, pp. 148–153, 1996.

[26] L. van Ginneken, "Buffer Placement in Distributed RC-tree Networks for Minimal Elmore Delay," *Proc. ISCAS*, pp. 865–868 vol.2, 1990.

[27] R. Bellman, *Dynamic Programming.* Dover Publications, N.Y, 1957.